

ORIGINAL ARTICLE

Structural, Optical, and Vibrational Properties of $(\text{Mn}_x\text{Mg}_{1-x}\text{Fe}_2\text{O}_4)$ Spinel Ferrites

Hasnain Ali^a, Fawad Ali^b, Shahbaz Afzal^{c,e}, Haneef Shah^{c,e}, Tahir Munir^{a,e}, Sakhi G. Sarwar^{d,e}, Adezuka Yahaya^g, Imosobomeh L. Ikhioya^{e,f,*}

^aInstitute of Physics, Baghdad ul Jadeed Campus, The Islamia University of Bahawalpur, Bahawalpur 63100, Pakistan.

^bNational Institute of Vacuum Science and Technology, Islamabad, 44000, Pakistan

^cDepartment of Physics, University of Education Lahore, DG Khan Campus 32200, Pakistan

^dCentre of Excellence in Solid-State Physics, University of the Punjab, Lahore, Pakistan

^eDepartment of Physics and Astronomy, University of Nigeria Nsukka, 410001, Nigeria

^fNational Centre for Physics, Quaid-i-Azam University Campus, Islamabad, 44000, Pakistan

^gDepartment of Physics, Federal College of Education, Okene, Kogi State, Nigeria

KEYWORDS

Spinel ferrites,
Magnetic materials,
Manganese-substituted ferrites,
Co-precipitation method

ARTICLE HISTORY

Received: September 30, 2023

Revised: July 11, 2023

Accepted: November 08, 2023

Published: February 13, 2024

ABSTRACT

The study explores the properties of $\text{Mn}_x\text{Mg}_{1-x}\text{Fe}_2\text{O}_4$ spinel ferrites. A detailed investigation of the structural, optical, and vibrational properties was carried out for the synthesized samples using X-ray diffraction (XRD), UV-visible spectroscopy, and Fourier Transform Infrared Spectroscopy (FTIR), respectively. Samples with varying Mn content were observed and their effects on material properties. XRD analysis revealed crystal structure and phase purity. UV spectroscopy was used for optical characteristics study. The vibrational modes and bonding characteristics of the synthesized spinel ferrites were examined using Fourier Transform Infrared (FTIR) spectroscopy. The outcomes shed light on the potential applications of $(\text{Mn}_x\text{Mg}_{1-x}\text{Fe}_2\text{O}_4)$ spinel ferrites in various technological fields, such as electronics, magnetics, and sensing applications. Spinel ferrites' properties can be changed using the co-precipitation synthesis method, which has shown promise.

1 Introduction

Spinel ferrites, a class of magnetic materials, have drawn a lot of interest because of their exceptional qualities and wide range of applications in numerous fields. Due to their distinct physical and chemical characteristics compared to larger particles or bulk, magnetic nanoparticles greatly interest scientists [1]–[3], [4]. Manganese ferrite (MnFe_2O_4) nanoparticles are magnetic nanoparticles that have the highest magnetic moment when compared to other ferrite systems [5].

Compared to CoFe_2O_4 and NiFe_2O_4 , MnFe_2O_4 has a significantly lower resistivity and a higher magnetic permeability. As a result, the addition of Mg ions changes the magnetic properties of manganese ferrite and increases the possibility of realizing superparamagnetic properties. This

condition gives rise to thermal energy at room temperature, preventing the anisotropy energy from returning to its low state. Since the sum of the magnetic moments of the magnetic material, except blocking temperature, are all pointing in different directions, the total magnetic moment of the bulk in this situation is zero. This intriguing property offers potential uses for a variety of electronic devices, including target materials for drug delivery systems and contrast agents in magnetic resonance imaging systems [6]–[11].

Numerous methods, including the coprecipitation method, sol-gel, microemulsion, hydrothermal, and others [12]–[16], have been developed to produce magnetic nanoparticles. The coprecipitation method is one of the best alternatives when weighed against alternative techniques because it is simple and efficient. This technique can be used in atmospheric conditions and results in a relatively narrow grain size distribution.

* CORRESPONDING AUTHOR | I. L. Ikhioya, ✉ imosobomeh.ikhioya@unn.edu.ng

© The Authors 2024. Published by JNMSR. This is an open access article under the CC BY-NC-ND license.

Chemicals with high-grade analysis qualifications are frequently used to produce magnetic nanoparticles. Iron sands (i.e., a plentiful supply of natural resources) are also present. e. with the highest hematite, magnetite, etc. content. (both on the coast and in the fine deposits of the river) can be found almost everywhere in Indonesia. Hematite content has also been reported to rise when materials are annealed at 800 °C under atmospheric conditions [17]. The tiny size of the fine sediment also makes it possible to extract it and use it as a starting point for the synthesis of magnetic nanoparticles.

The $(\text{Mn}_x\text{Mg}_{1-x}\text{Fe}_2\text{O}_4)$ spinel ferrites synthesized using the co-precipitation method are examined in this paper. Spinel's properties can be customized for various technological applications by replacing Mn in its lattice. Better magnetic materials could be made if we knew more about how spinel ferrites work.

The study aims to examine the properties of magnetic materials. The samples' structural, optical, and vibrational properties are assessed using X-ray diffraction, UV-visible spectroscopy, and FTIR. This study adds to the growing body of knowledge in functional materials by shedding light on the structural, optical, and vibrational characteristics of $(\text{Mn}_x\text{Mg}_{1-x}\text{Fe}_2\text{O}_4)$ spinel ferrites produced by the co-precipitation technique, opening the door for future developments in spinel ferrite-based technology.

2 Materials and methods

The natural iron-sand, from Kata Beach in West Sumatera, is one of $\text{Mn}_x\text{Mg}_{1-x}\text{Fe}_2\text{O}_4$'s main constituents. As a result, MnCl_2 and MgCl_2 provide Mn^{2+} and Mg^{2+} ions. The values chosen for the stoichiometric x are 0.25, 0.50, 0.75, and 1. In the beginning, 5 mL of HCl was used to dissolve 8 grams of iron sand. After the solution has been filtered using Whatman Paper No. 42, Mn^{2+} and Mg^{2+} are added in amounts equal to stoichiometry and stirred until the mixture is homogeneous. In addition, the solution is added to 100 ml of a 2 M NH_4OH solution and stirred continuously for two hours at 110 °C using a 200 rpm magnetic stirrer. The precipitated yield is dried overnight and repeatedly washed with ethanol and deionized water to produce a clean product. The final product is therefore dried in an oven set to 70 °C.

3 Results and Discussions

3.1 X-Ray Diffraction Technique

The powder X-ray diffraction (PXRD) measurements are performed to confirm the crystallographic structure, phase purity, and identification of the synthesized samples of the pure and manganese-doped magnesium ferrites $\text{Mn}_x\text{Mg}_{1-x}\text{Fe}_2\text{O}_4$. The variable composition "x" ranges from 0 to 1. XRD pattern gives valuable information about crystallographic properties.

Upon analyzing the XRD pattern of $\text{Mn}_x\text{Mg}_{1-x}\text{Fe}_2\text{O}_4$, a series of distinct diffraction peaks are usually seen. Such peaks offer insights into the atomic arrangement of the material.

Examining the positions, intensities, and shapes can determine the crystal structure and composition. The diffraction peaks' strength reveals the abundance of crystallographic phases in the sample. This aids in determining crystallinity and evaluating the synthesized material's quality.

The PXRD patterns at different molarities are recorded in the range 20°–70° and are exhibited in Figure 1 (a–e). The primary diffraction (2θ) intensity peaks values of MgFe_2O_4 and $\text{Mn}_{0.25}\text{Mg}_{0.75}\text{Fe}_2\text{O}_4$ NPs present similar patterns at 30.12°, 35.40°, 43.19°, 53.76°, 62.04°, corresponding to (220), (311), (400), (422), and (440) crystal planes.

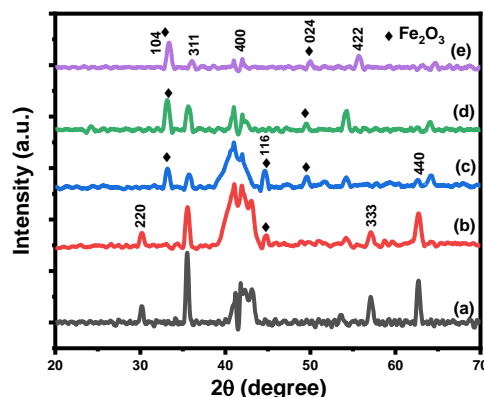


Figure 1: XRD pattern for (a) MgFe_2O_4 , (b) $\text{Mn}_{0.25}\text{Mg}_{0.75}\text{Fe}_2\text{O}_4$, (c) $\text{Mn}_{0.50}\text{Mg}_{0.50}\text{Fe}_2\text{O}_4$, (d) $\text{Mn}_{0.75}\text{Mg}_{0.25}\text{Fe}_2\text{O}_4$, and (e) MnFe_2O_4

These observed patterns are very much consistent with the metal ferrite oxides (MFO) NPs cubic spinel phase (JCPDS Card No. 88–1943) [18]. The diffraction peak observed at 57.16° resembles the manganese hkl plane of (333) and is in good agreement with (ICDD Card No. 01-074-2403) [19], confirming manganese impurity in the lattice of MgFe_2O_4 . As the concentration is varied beyond, the diffraction peaks at 30.09° and 57.16° seem to have disappeared and are not present in any of the samples and can be correlated to the changing of the molarity concentrations.

However, very distinct diffraction peaks of Fe_2O_3 were also recorded and were well matched with (JCPDS Card No. 05-0566). These findings are consistent with the existing literature [20], [21]. The shifting in diffraction angle $2\theta = 53.76^\circ$ towards a higher value with changing molarity was also found. An absence of any extra peak in the diffraction patterns is clear of the phase purity.

The average crystallite size (D) is evaluated by the Scherrer equation [22], [27]–[37]:

$$D = \frac{k\lambda}{\beta \cos \theta} \quad (1)$$

where λ stands for the wavelength of the incident X-ray beam, k is a shape factor and is taken as 0.9, full width at half maximum of broadened characteristic peaks, and Bragg

diffraction angle are represented by β and θ are, respectively. The value of D for MgFe_2O_4 , $\text{Mn}_{0.25}\text{Mg}_{0.75}\text{Fe}_2\text{O}_4$, $\text{Mn}_{0.50}\text{Mg}_{0.50}\text{Fe}_2\text{O}_4$, $\text{Mn}_{0.75}\text{Mg}_{0.25}\text{Fe}_2\text{O}_4$, and MnFe_2O_4 NPs is determined to be 18.02, 13.26, 10.58, 15.35, and 15.34 nm.

The table of XRD measurements presents important data about the crystalline features of a substance, including 2θ , interplanar distance, hkl values, FWHM, and crystallite size, as can be seen in Table 1.

Table 1: Structural parameters calculated using XRD data

$\text{Mn}_x\text{Mg}_{1-x}\text{Fe}_2\text{O}_4$	Peak position (2θ)	(hkl)	FWHM (β)	Crystallite Size, D (nm)	Average D (nm)		
x = 0	30.17	220	0.34418	21.75694816	18.02160851		
	35.52	311	0.36103	20.45798649			
	43.11	400	0.49329	14.6225838			
	53.53	422	0.34814	19.89037377			
	57.16	333	0.46808	14.54995356			
	62.6	440	0.39324	16.8518053			
x = 0.25	30.18	220	0.42927	17.44349889	13.26009414		
	35.54	311	0.45976	16.06351167			
	43.94	400	0.82747	8.691715061			
	51.21	024	0.30926	22.6144574			
	53.52	422	4.70235	1.487287653			
	57.12	333	0.53158	12.81405106			
x = 0.50	62.7	440	0.63812	10.3791536	10.58835738		
	33.21	104	0.44729	16.61591293			
	35.54	311	0.47769	15.46057093			
	43.94	400	0.82456	8.72238947			
	45.23	116	4.60532	1.554556183			
	50.23	024	0.41223	16.9656432			
	53.53	422	0.38396	18.03478155			
	57.12	333	0.68756	9.907052858			
	62.7	440	0.32644	20.28901328			
	x = 0.75	33.23	104	0.45761		16.24034606	15.35521589
		35.55	311	0.46721		15.80729709	
		43.96	400	0.38753		18.55815206	
50.23		024	0.52431	13.39346693			
53.57		422	0.62674	11.04671022			
57.6		333	0.44729	15.19427252			
x = 1	62.74	440	0.38396	17.24626634	15.34469142		
	33.25	104	0.45761	16.23950001			
	35.55	311	0.46721	15.80729709			
	43.96	400	0.38753	18.55815206			
	51.23	024	0.52431	13.33816971			
	53.57	422	0.62674	11.04671022			
	57.84	333	0.44729	15.17674447			
	62.74	440	0.38396	17.24626634			

3.2 UV-Vis Spectroscopy

The UV-vis absorption spectrum of $\text{MnMgFe}_2\text{O}_4$, a spinel ferrite compound, is investigated using a spectrophotometer in the different wavelength ranges. The absorption spectrum helps us understand the material's light and electronic properties.

The UV-visible absorption spectrum displays absorbance plots of $\text{MnMgFe}_2\text{O}_4$ nanoparticles at various molarities as presented in Figure 2 (a). It can be seen that all of the produced nanoparticles showed a similar pattern in the absorbance plot in the UV region and an increase in absorbance is recorded for

the $\text{Mn}_{0.25}\text{Mg}_{0.75}\text{Fe}_2\text{O}_4$ and $\text{Mn}_{0.50}\text{Mg}_{0.50}\text{Fe}_2\text{O}_4$ samples as the wavelength moved from 300 – 350 nm in the UV region. Compared to MgFe_2O_4 , it is discovered that adding a small amount of Mn (0.25 & 0.50) increases the absorbance throughout the electromagnetic spectrum. However, beyond the (0.25 & 0.50 of Mn), further increases in the dopant (to 0.75 & 1.0 of Mn) reduce the absorbance data. The absorbance of the material seems to vary with changing Mn molar concentration. The spectrum shows distinct absorption bands in the UV region.

In the UV region (300 – 350 nm), a broad absorption band is observed, showing electronic transitions involving the valence and conduction bands. This absorption is likely attributed to

charge transfer transitions between the metal ions in the spinel structure.

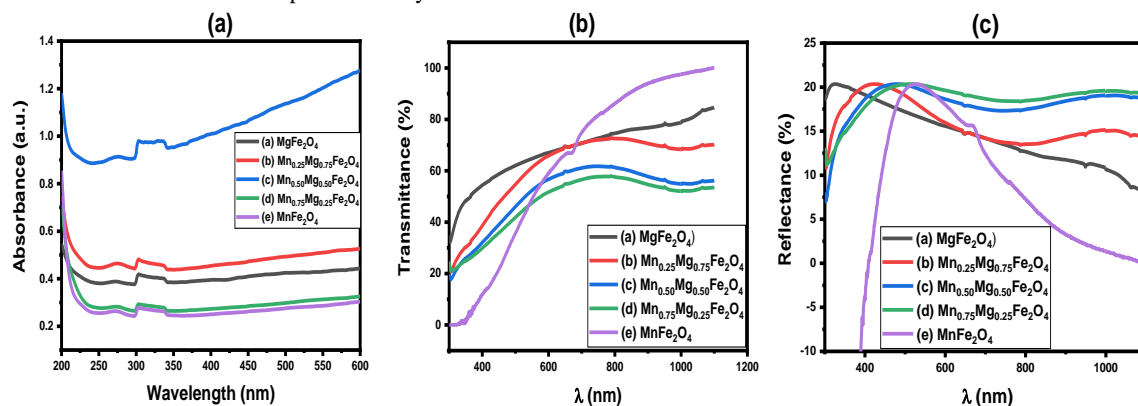


Figure 2: UV-vis spectra of (a) $MgFe_2O_4$, (b) $Mn_{0.25}Mg_{0.75}Fe_2O_4$ (c) $Mn_{0.50}Mg_{0.50}Fe_2O_4$ (d) $Mn_{0.75}Mg_{0.25}Fe_2O_4$ and (e) $MnFe_2O_4$

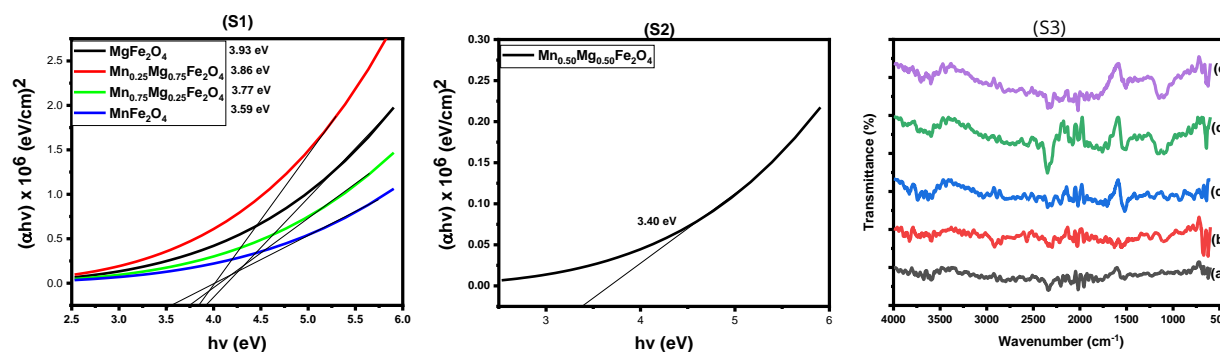


Figure 3: (S1) Band gap energy values of $MgFe_2O_4$, $Mn_{0.25}Mg_{0.75}Fe_2O_4$, $Mn_{0.75}Mg_{0.25}Fe_2O_4$ and $MnFe_2O_4$ (S2) $Mn_{0.50}Mg_{0.50}Fe_2O_4$ (S3) FTIR spectra of (a) $MgFe_2O_4$ (b) $Mn_{0.25}Mg_{0.75}Fe_2O_4$ (c) $Mn_{0.50}Mg_{0.50}Fe_2O_4$ (d) $Mn_{0.75}Mg_{0.25}Fe_2O_4$ (e) $MnFe_2O_4$

The observed absorption bands can be attributed to the crystal field splitting and exchange interactions between the transition metal ions in the spinel structure. Overall, $Mn_{0.50}Mg_{0.50}Fe_2O_4$ has a strong UV absorbance, which makes the material appropriate for p-n junction formation in solar cells and photovoltaic applications.

Notably, as the UV wavelength increases from 400 to 450 nm, a rise in transmittance is seen for the $MgFe_2O_4$ and $Mn_{0.25}Mg_{0.75}Fe_2O_4$ samples. However, the greatest increase is observed in the sample $MnFe_2O_4$ as shown in Figure 2(b). Similarly, Figure 2(c) displays the reflectance plots of $MnMgFe_2O_4$ nanoparticles at different molarities. All produced nanoparticles are found to follow the same pattern in the UV region of the reflectance spectra. However, the reflectance of $MnFe_2O_4$ seemed to decrease at the increasing wavelengths.

The energy band gap (E_g) of $MgFe_2O_4$ at varied dopant molarities is deduced via Equation (2):

$$(\alpha hv)^2 = A(hv - E_g) \quad (2)$$

Where α^2 is absorption coefficient square, hv is photon energy, and E_g is the energy band gap [22]. Figure 3(S1 and S2) shows a plot of $(\alpha hv)^2$ against hv at varied molarities. The materials'

energy band gap is calculated from this plot by projecting the straight section of the curve down to the hv axis at $(\alpha hv)^2 = 0$. $MgFe_2O_4$, $Mn_{0.25}Mg_{0.75}Fe_2O_4$, $Mn_{0.75}Mg_{0.25}Fe_2O_4$, and $MnFe_2O_4$ exhibit a band gap energy of 3.93, 3.86, 3.77, 3.59 eV, however, $Mn_{0.50}Mg_{0.50}Fe_2O_4$ reveals the lowest band gap of 3.40 eV. Different molarity concentrations have a significant influence on the energy gap, as evidenced in the report.

3.3 Fourier Transform Infrared Spectroscopy (FTIR)

The molecular vibrations and functional groups in $Mn_xMg_{1-x}Fe_2O_4$ are analyzed using the potent analytical technique known as FTIR spectroscopy, where x denotes the changing amounts of manganese (Mn) and magnesium (Mg) in the spinel structure as shown in Figure 3(S3). Using a high-resolution FTIR spectrometer, the data is collected in the range of 600 – 4000 cm^{-1} , and the observations are made under natural lighting.

It can be seen that the $Mn_xMg_{1-x}Fe_2O_4$ spectra show several distinctive absorption bands in the infrared spectrum. The vibrational modes of the atoms and functional groups that make up the spinel structure can be studied from these bands. The tetrahedral and octahedral complexes' stretched vibrations are thought to be responsible for the absorption band at about ~600 [23]. Around 3399 and 1625 cm^{-1} are where the stretching and

bending vibrations of hydroxyl groups and H₂O are found, respectively [24]. The spectra of FTIR in the range 900 – 600 cm⁻¹ confirmed the production of spinel ferrites [25]. The metal and oxygen bonds are also found in this range. The absorption band found at 1550 cm⁻¹ suggests that there are some citrates present in the ferrite pores [26].

4 Conclusions

We have successfully synthesized Mn_xMg_{1-x}Fe₂O₄ nanoparticles. The primary diffraction (2θ) intensity peaks values of MgFe₂O₄ and Mn_{0.25}Mg_{0.75}Fe₂O₄ NPs present similar patterns at 30.12°, 35.40°, 43.19°, 53.76°, 62.04°, corresponding to (220), (311), (400), (422), and (440) crystal planes. These observed patterns are very much consistent with the MFO NP cubic spinel phase. It can be seen that all of the produced nanoparticles showed a similar pattern in the absorbance plot in the UV region and an increase in absorbance is recorded for the Mn_{0.25}Mg_{0.75}Fe₂O₄ and Mn_{0.50}Mg_{0.50}Fe₂O₄ samples as the wavelength moved from 300 – 350 nm in the UV region. Compared to MgFe₂O₄, it is discovered that adding a small amount of Mn (0.25 & 0.50) increases the absorbance throughout the electromagnetic spectrum. However, beyond the (0.25 & 0.50 of Mn), further increases in the dopant (to 0.75 & 1.0 of Mn) reduce the absorbance data. The absorbance of the material seems to vary with changing Mn molar concentration. The spectrum shows distinct absorption bands in the UV region. MgFe₂O₄, Mn_{0.25}Mg_{0.75}Fe₂O₄, Mn_{0.75}Mg_{0.25}Fe₂O₄, and MnFe₂O₄ exhibit a band gap energy of 3.93, 3.86, 3.77, 3.59 eV, however, Mn_{0.50}Mg_{0.50}Fe₂O₄ reveals the lowest band gap of 3.40 eV. The statistics unambiguously show that varying molarity concentration changes the energy gap significantly.

Acknowledgment

We appreciate the immense contribution of all the authors to the success of the research.

Authors' Credit Statement

Hasnain Ali, Fawad Ali, Shahbaz Afzal, Haneef Shah: Writing and editing original draft, Methodology, Conceptualization; **Tahir Munir, Sakhi G. Sarwar:** Data collection and Data curation; **Adezuka Yahaya and Imosobomeh L. Ikhioya:** Investigation and Visualization.

Declaration of Competing Interest

The authors declare no personal or financial conflicts that may influence the research presented in this paper.

References

[1] S. J. Salih and W. M. Mahmood, "Review on magnetic spinel ferrite (MFe₂O₄) nanoparticles: From synthesis

to application," *Heliyon*, vol. 9, no. 6, p. e16601, 2023, doi: 10.1016/j.heliyon.2023.e16601.

- [2] F. G. da Silva, J. Depeyrot, A. F. C. Campos, R. Aquino, D. Fiorani, and D. Peddis, "Structural and Magnetic Properties of Spinel Ferrite Nanoparticles," *Journal of Nanoscience and Nanotechnology*, vol. 19, no. 8, pp. 4888–4902, 2019, doi: 10.1166/jnn.2019.16877.
- [3] H. Saqib, S. Rahman, R. Susilo, B. Chen, and N. Dai, "Structural, vibrational, electrical, and magnetic properties of mixed spinel ferrites Mg_{1-x}Zn_xFe₂O₄ nanoparticles prepared by co-precipitation," *AIP Advances*, vol. 9, no. 5, 2019, doi: 10.1063/1.5093221.
- [4] E. Suharyadi, E. A. Setiadi, N. Shabrina, T. Kato, and S. Iwata, "Magnetic properties and microstructures of polyethylene glycol (PEG)- coated cobalt ferrite (CoFe₂O₄) nanoparticles synthesized by coprecipitation method," *Adv Mat Res*, vol. 896, pp. 126–133, 2014, doi: 10.4028/www.scientific.net/AMR.896.126.
- [5] R. K. Kotnala and J. Shah, *Ferrite Materials: Nano to Spintronics Regime*, vol. 23. Elsevier, 2015. doi: 10.1016/B978-0-444-63528-0.00004-8.
- [6] S. Singh, H. Chawla, A. Chandra, and S. Garg, "Magnetic hybrid nanoparticles for drug delivery," *Magnetic Nanoparticle-Based Hybrid Materials: Fundamentals and Applications*, vol. 2, no. 3, pp. 319–342, 2021, doi: 10.1016/B978-0-12-823688-8.00034-X.
- [7] I. Larraza, M. López-González, T. Corrales, and G. Marcelo, "Hybrid materials: Magnetite-Polyethylenimine-Montmorillonite, as magnetic adsorbents for Cr(VI) water treatment," *J Colloid Interface Sci*, vol. 385, no. 1, pp. 24–33, 2012, doi: 10.1016/j.jcis.2012.06.050.
- [8] F. Saoud, "Superparamagnetic nanoparticles for synthesis and purification of polymers prepared via controlled/" living" radical polymerization (CLRP)." Stellenbosch: University of Stellenbosch, 2010.
- [9] M. Anbarasu, M. Anandan, E. Chinnasamy, V. Gopinath, and K. Balamurugan, "Synthesis and characterization of polyethylene glycol (PEG) coated Fe₃O₄ nanoparticles by chemical co-precipitation method for biomedical applications," *Spectrochim Acta A Mol Biomol Spectrosc*, vol. 135, pp. 536–539, 2015, doi: 10.1016/j.saa.2014.07.059.
- [10] B. Feng et al., "Synthesis of Fe₃O₄/APTES/PEG diacid functionalized magnetic nanoparticles for MR imaging," *Colloids Surf A Physicochem Eng Asp*, vol. 328, no. 1–3, pp. 52–59, 2008, doi: 10.1016/j.colsurfa.2008.06.024.
- [11] Wahajuddin and S. Arora, "Superparamagnetic iron oxide nanoparticles: Magnetic nanoplatforms as drug carriers," *Int J Nanomedicine*, vol. 7, pp. 3445–3471, 2012, doi: 10.2147/IJN.S30320.

- [12] S. Hcini, A. Selmi, H. Rahmouni, A. Omri, and M. L. Bouazizi, "Structural, dielectric and complex impedance properties of $T_{0.6}Co_{0.4}Fe_2O_4$ (T=Ni, Mg) ferrite nanoparticles prepared by sol gel method," *Ceram Int*, vol. 43, no. 2, pp. 2529–2536, 2017, doi: 10.1016/j.ceramint.2016.11.055.
- [13] Y. F. Shen, J. Tang, Z. H. Nie, Y. D. Wang, Y. Ren, and L. Zuo, "Tailoring size and structural distortion of Fe_3O_4 nanoparticles for the purification of contaminated water," *Bioresour Technol*, vol. 100, no. 18, pp. 4139–4146, 2009, doi: 10.1016/j.biortech.2009.04.004.
- [14] X. Liang, H. Shi, X. Jia, Y. Yang, and X. Liu, "Dispersibility, Shape and Magnetic Properties of Nano- Fe_3O_4 Particles," *Materials Sciences and Applications*, vol. 02, no. 11, pp. 1644–1653, 2011, doi: 10.4236/msa.2011.211219.
- [15] Q. Chen, A. J. Rondinone, B. C. Chakoumakos, and Z. John Zhang, "Synthesis of superparamagnetic $MgFe_2O_4$ nanoparticles by coprecipitation," *J Magn Magn Mater*, vol. 194, no. 1, pp. 1–7, 1999, doi: 10.1016/S0304-8853(98)00585-X.
- [16] J. Kis-Csitári, Z. Kónya, and I. Kiricsi, "Sonochemical synthesis of inorganic nanoparticles," *NATO Science for Peace and Security Series B: Physics and Biophysics*, vol. 6, no. August, pp. 369–372, 2008, doi: 10.1007/978-1-4020-8903-9-33.
- [17] B. Purnama, R. Kusuma, B. Legowo, Suharyana, and A. T. Wijayanta, "Identification of magnetic minerals in the fine-grain sediment on the Bengawan Solo River," *IOP Conf Ser Mater Sci Eng*, vol. 333, no. 1, 2018, doi: 10.1088/1757-899X/333/1/012017.
- [18] R. Elangovan, V. Vijayan, S. Bakthavatsalam, K. Ramkumar, T. Sathish, and K. Sudhakar, "A Facile Synthesis of $MgFe_2O_4/ZnS$ Heterojunction with Effectively Enhanced Visible Light Photocatalytic Activity for Degradation of Methylene Blue and Crystal Violet Dyes," *J Clust Sci*, vol. 34, no. 2, pp. 991–999, 2022, doi: 10.1007/s10876-022-02271-0.
- [19] K. Kombaiah et al., "A Green approach: synthesis, characterization and opto-magnetic properties of $Mg_xMn_{1-x}Fe_2O_4$ spinel nanoparticles," *Journal of Materials Science: Materials in Electronics*, vol. 28, no. 14, pp. 10321–10329, 2017, doi: 10.1007/s10854-017-6800-2.
- [20] M. Tadic et al., "Magnetic properties of hematite (α - Fe_2O_3) nanoparticles synthesized by sol-gel synthesis method: The influence of particle size and particle size distribution," *Journal of Electrical Engineering*, vol. 70, no. 7, pp. 71–76, 2019, doi: 10.2478/jee-2019-0044.
- [21] M. Qayoom, K. A. Shah, A. H. Pandit, A. Firdous, and G. N. Dar, "Dielectric and electrical studies on iron oxide (α - Fe_2O_3) nanoparticles synthesized by modified solution combustion reaction for microwave applications," *J Electroceram*, vol. 45, no. 1, pp. 7–14, 2020, doi: 10.1007/s10832-020-00219-2.
- [22] S. Afzal, S. Tehreem, T. Munir, S. G. Sarwar, and I. L. Ikhioya, "Impact of Transition Metal Doped Bismuth Oxide Nanocomposites on the Bandgap Energy for Photoanode Application," vol. 2, no. 1, pp. 104–109, 2023.
- [23] V. M. Khot, A. B. Salunkhe, M. R. Phadatare, N. D. Thorat, and S. H. Pawar, "Low-temperature synthesis of $Mn_xMg_{1-x}Fe_2O_4$ ($x = 0-1$) nanoparticles: Cation distribution, structural and magnetic properties," *J Phys D Appl Phys*, vol. 46, no. 5, 2013, doi: 10.1088/0022-3727/46/5/055303.
- [24] J. K. Rajput, P. Arora, G. Kaur, and M. Kaur, " $CuFe_2O_4$ magnetic heterogeneous nanocatalyst: Low power sonochemical-coprecipitation preparation and applications in synthesis of 4H-chromene-3-carbonitrile scaffolds," *Ultrason Sonochem*, vol. 26, pp. 229–240, 2015, doi: 10.1016/j.ultrsonch.2015.01.008.
- [25] G. Padmapriya, A. Manikandan, V. Krishnasamy, S. K. Jaganathan, and S. A. Antony, "Enhanced Catalytic Activity and Magnetic Properties of Spinel $Mn_xZn_{1-x}Fe_2O_4$ ($0.0 \leq x \leq 1.0$) Nano-Photocatalysts by Microwave Irradiation Route," *J Supercond Nov Magn*, vol. 29, no. 8, pp. 2141–2149, 2016, doi: 10.1007/s10948-016-3527-x.
- [26] G. Xian et al., "Synthesis of Spinel Ferrite MFe_2O_4 ($M = Co, Cu, Mn, \text{ and } Zn$) for Persulfate Activation to Remove Aqueous Organics: Effects of M-Site Metal and Synthetic Method," *Front Chem*, vol. 8, no. March, pp. 1–11, 2020, doi: 10.3389/fchem.2020.00177.
- [27] A. U. Agobi et al., "Optical and structural properties of graphene oxide-incorporated polyvinylpyrrolidone/copper ternary nanocomposites (PVP/Cu/GO) films," *Rev. Mex. Fis.*, vol. 69, no. 3, pp. 1–9, 2023, doi: 10.31349/RevMexFis.69.031001.
- [28] A. Ali, S. Afzal, T. Khaleeq, H. Shah, M. Usman, and L. Imosobomeh, "Synthesis and Characterization of Chitosan-Silver Nanocomposite Using Chemical Reduction Method and their Antibacterial Properties," vol. 2, no. 1, pp. 117–122, 2023.
- [29] I. L. Ikhioya, S. O. Aisida, I. Ahmad, and F. I. Ezema, "The effect of molybdenum dopant on rare earth metal chalcogenide material," *Chem. Phys. Impact*, vol. 7, no. April, p. 100269, 2023, doi: 10.1016/j.chphi.2023.100269.
- [30] I. L. Ikhioya and A. C. Nkele, "Results in Optics Properties of electrochemically-deposited NiTe films doped with molybdenum at varying temperatures," *Results Opt.*, vol. 12, no. April, p. 100494, 2023, doi: 10.1016/j.rio.2023.100494.
- [31] I. L. Ikhioya and A. C. Nkele, "Results in Optics A novel synthesis of hydrothermally-prepared yttrium

- selenide and erbium selenide nanomaterials doped with magnesium,” *Results Opt.*, vol. 13, no. September, p. 100555, 2023, doi: 10.1016/j.rio.2023.100555.
- [32] I. L. Ikhioya et al., “Asian Journal of Nanoscience and Original Research Article Impact of precursor temperature on physical properties of molybdenum doped nickel telluride metal chalcogenide material,” vol. 2, pp. 156–167, 2023, doi: 10.26655/AJNANOMAT.2023.2.5.
- [33] E. N. Josephine, O. S. Ikponmwosa, and I. L. Ikhioya, “Asian Journal of Nanoscience and Original Research Article Enhanced physical properties of SnS / SnO semiconductor material,” vol. 3, pp. 199–212, 2023, doi: 10.26655/AJNANOMAT.2023.3.3.
- [34] E. O. Ojegu, O. B. Odia, M. O. Osiele, A. E. Godfrey, and I. L. Ikhioya, “Effect of precursor temperature on electrochemically deposited zirconium doped chromium telluride using a standard three-electrode system,” vol. 14, no. 11, pp. 1148–1159, 2023.
- [35] S. O. Samuel, M. F. Lagbegha-ebi, E. P. Ogherohwo, and I. L. Ikhioya, “Improve physical properties of zirconium doped strontium sulphide for optoelectronic purpose,” *Results Opt.*, vol. 13, no. June, p. 100518, 2023, doi: 10.1016/j.rio.2023.100518.
- [36] H. Shah, S. Afzal, M. Usman, K. Shahzad, and I. L. Ikhioya, “Impact of Annealing Temperature on Lanthanum Erbium Telluride (La_{0.1}Er_{0.2}Te_{0.2}) Nanoparticles Synthesized via Hydrothermal Approach,” *Adv. J. Chem. Sect. A*, vol. 6, no. 4, pp. 342–351, 2023, doi: 10.22034/AJCA.2023.407424.1386.
- [37] K. I. Udofia, I. L. Ikhioya, D. N. Okoli, and J. Azubike, “Asian Journal of Nanoscience and Original Research Article Impact of doping on the physical properties of PbSe chalcogenide material for photovoltaic application,” vol. 2, pp. 135–147, 2023, doi: 10.26655/AJNANOMAT.2023.2.3.